Int. J. Heat Mass Transfer. Vol. 36, No. 18, pp. 4443–4453, 1993
Printed in Great Britain

0017–9310/93 $6.00 + 0.00

Unsteady mixed convection heat transfer from a solid sphere: the conjugate problem

HOA D. NGUYEN,† SEUNGHO PAIK† and JACOB N. CHUNG‡

† Idaho National Engineering Laboratory, EG&G Idaho, Inc., Idaho Falls, ID 83415, U.S.A.
‡ Department of Mechanical and Materials Engineering, Washington State University, Pullman, WA 99164, U.S.A.

(*Received* 3 *August* 1992 *and in final form* 11 *May* 1993)

Abstract—Heat transfer associated with a spherical particle under simultaneous free and forced convection is numerically investigated using a combined Chebyshev Legendre spectral method. Both internal and external thermal resistances are taken into consideration by means of a conjugate model consisting of the full Navier–Stokes equations for external flow and the energy equations for both inside and outside the sphere. An influence matrix technique is employed to resolve the difficulties created by the lack of vorticity boundary conditions and to decouple the energy equations from interfacial couplings. Simulation results reveal that effects due to natural convection are most remarkable in the wake where the flow structure is changed. The overall Nusselt number and the drag coefficient show an increase or decrease in magnitude depending on whether gravity-induced flow aids or opposes the main flow. However, the change does not exceed 17% for the cases $Gr/Re^2 \leqslant 40$. When the buoyancy and the free stream are in the same direction, the effects are less pronounced than when they are in the opposite direction.

1. INTRODUCTION

LITERATURE concerning heat transfer associated with a spherical particle is numerous (see Clift *et al.* [1]). Two particular areas which received a great deal of theoretical and experimental investigations have been forced and free convection. In the former, the convective mode of heat transfer is primarily controlled by an external forcing mechanism which causes a relative motion between the particle and its surroundings. Detailed analysis of this situation can be found in Dennis *et al.* [2] and Paik *et al.* [3]. In free convection, the motion in the participating medium is driven by the buoyancy force as a consequence of density variation which, in turn, is induced by thermal non-equilibrium. Representative works in this area include Riley [4], Fujii *et al.* [5, 6], Ingham [7], and Geoola and Cornish [8]. Both scenarios just described are actually the limiting cases under which one type of convection is predominant over the other. In many cases, however, both forced and free convection are of the same order of magnitude; therefore, both must be accounted for in the model.

Modeling a mixed convective heat transfer problem can be tedious because of the strong couplings between the energy and momentum equations. Three classes of solutions have appeared in the literature. They are the perturbation solution, boundary layer solution, and direct numerical solution. In the perturbation approach [9], the governing equations are linearized according to the matched asymptotic expansions of the perturbation theory so that analytical solutions to the first few order terms are possible. Even with the first few order terms, most of the physics of the problem are contained in the solution as long as the perturbed quantities, the Reynolds (Re) and the Grashof (Gr) numbers in this case, are small. In the boundary layer approach, the energy and momentum equations are simplified using the boundary layer approximation and are converted to a system of ordinary equations through the similarity transformation [10, 11]. As usual, the solution here is valid if and only if there exists thin thermal and hydrodynamic boundary layers along the sphere surface which is the case when Pe (Peclet) and Re are large. Granted that this condition holds, the solution still fails to give the correct picture of the transport process beyond the point of separation. Besides those shortcomings, the aforementioned methodologies cover only a limited range of conditions that one often encounters in practice. It is clear that a more general approach is needed and undoubtedly computer modeling is the answer. One of the early attempts in solving this problem was due to Wong *et al.* [12] who numerically solved the problem by the finite element method. Several important features were revealed from their study. In particular, the surface pressure decreases significantly near the rear stagnation point and increases, to a lesser extent, near the front stagnation point as Gr increases. Substantial increase is also found in the local shear stress as well as the heat transfer rate. These effects are primarily due to the buoyancy force that accelerates the flow near the sphere surface. Despite the fact that the problem is relatively well understood, all the above investigations neglected the transient effects and assumed a negligible transfer resistance within the sphere. According to a study of Oliver and Chung [13], neglecting the internal transport resistance would result in overprediction of the Nusselt number unless the volu-

NOMENCLATURE

a expansion coefficient for vorticity
b expansion coefficient for stream function
$c, \tilde{c}$ expansion coefficients for exterior and interior temperatures, respectively
C_D drag coefficient
C_p heat capacity
$\mathbf{e}$ unit vector associated with spherical coordinates
g gravitational constant
$\hat{G}^{(1)}_{k,l}, \hat{G}^{(2)}_{k,l}$ Chebyshev matrix for first and second derivative, respectively
Gr Grashof number
H_{nk} see equation (25)
I see equation (17)
Nu Nusselt number
NL number of terms retained in the Legendre expansion
$NT+1$ number of collocation points
P_n Legendre polynomial of order n
$P^1_n, P^2_n, \ldots$ associated Legendre function of the first kind, second kind, etc., and of order n
Pe Peclet number
r radial coordinate
R sphere radius
Re Reynolds number
S_{nk} see equation (24)
t dimensional time
T_i Chebyshev polynomial of order i
$\mathbf{u}$ local velocity vector
U_∞ free stream velocity
z $\cos\theta$
Z dimensionless temperature.

Greek symbols

α thermal diffusivity
β isothermal expansion coefficient
γ product of 3-J coefficients, see equation (29)
δ_{ij} Kronecker delta
$\Delta\tau$ time increment
$\{\varepsilon\}$ tolerance vector
ζ dimensionless vorticity
η coordinate transformation, see equation (17)
θ angular coordinate measured in radians
λ product of 3-J coefficients, see equation (28)
μ dynamic viscosity
ν kinematic viscosity
ξ coordinate transformation, see equation (17)
Ξ_0, Ξ_1 auxiliary functions, see equation (30)
Π fluid pressure
ρ density
τ dimensionless time
Φ ratio of the transport coefficient of the inside to outside
χ product of 3-J coefficients, see equation (27)
ψ dimensionless stream function
ω product of 3-J coefficient, see equation (26).

Superscript

m iteration level.

Subscripts

b pertains to volume-averaged quantity
conj conjugate problem
ext external problem
int internal problem
m pertains to mean quantity
s pertains to sphere surface
∞ pertains to free stream condition
0 pertains to initial condition.

metric heat capacity ratio of the sphere to the external fluid is large ($(\tilde{\rho}\tilde{C}_p/\rho C_p) \gg 1$). As the system departs from this condition, the surface temperature fails to remain constant and more importantly it is not known a priori; hence, the problem must be formulated in a conjugate manner. In this fashion, the governing equations of both continuous and dispersed phases, the appropriate asymptotic conditions at the far field and at the sphere center, and the continuity of temperature and of heat flux at the surface would form a well-posed formalism of the heat transfer problem associated with a spherical particle.

The purpose of this article is three-fold. First, a rigorous mathematical treatment is used to describe the heat transfer process for systems in the intermediate range of volumetric heat capacity ratio. Second, transient effects are included so that temporal evolution of the flow and temperature fields can be predicted. Third, a spectral numerical scheme is devised to deal with the conjugate problems. Physically, the present paper differs from the work of Wong *et al.* [12] in two aspects that internal thermal resistance and transient effects are also incorporated. With regard to the last objective, it is our continuing effort to develop a combined Galerkin-collocation spectral numerical method, which has successfully been applied to the flow equation [14], for coupled viscous flow and heat transfer problems.

2. MATHEMATICAL FORMULATION

2.1. *Problem statement*

Consider a solid particle, assumed to be spherical in shape, of radius R suspended in an unbounded convective environment with a uniform velocity U_∞ as sketched in Fig. 1. Initially, the particle is at temperature Z_0 and is hotter than the host medium which is maintained at temperature Z_∞. Due to the thermal potential difference, heat flows from the particle to the surrounding fluid as dictated by the second law of thermodynamics. As a result of the absorption of energy, fluid particles in the proximity of the hot sphere become warmer causing a density variation which, in turn, creates a motion in the direction opposite to the gravity and is driven by the gravitational interaction. This gravity-induced flow when superimposed on the pre-existing motion would modify the flow field, hence the temperature field, especially in the wake region. Depending on the direction of the sphere motion and the buoyancy, this forcing mechanism could aid or oppose the main flow and could produce dominant effects.

In view of the complexities in the present investigation, we shall formulate the problem with the following assumptions: (i) the fluid is Newtonian with constant properties except density which varies as a direct consequence of change in temperature, (ii) the transport processes are axisymmetric and without radiative interactions, (iii) the Boussinesq approximation is valid, and (iv) the line of action of gravity is parallel to the free stream velocity.

2.2. *Governing equations*

Under the scenario outlined above, the heat transfer process is governed by the conservation of mass, momentum, and energy. These laws give rise to the following equations whose dimensionless form may be cast in spherical coordinates as

$$\frac{\partial \zeta}{\partial \tau} - \frac{1}{r}\frac{\partial(\psi, \zeta/r\sin\theta)}{\partial(r,\theta)} = \frac{2}{Re}\frac{1}{r\sin\theta}E^2(\zeta r\sin\theta) + \frac{Gr}{Re^2}\left[\sin\theta\frac{\partial Z}{\partial r} + \frac{\cos\theta}{r}\frac{\partial Z}{\partial \theta}\right], \quad (1)$$

$$E^2\psi = -\zeta r\sin\theta, \quad (2)$$

$$\frac{\partial Z}{\partial \tau} + u_r\frac{\partial Z}{\partial r} + \frac{u_\theta}{r}\frac{\partial Z}{\partial \theta} = \frac{2}{Pe}\left[\frac{1}{r^2}\frac{\partial}{\partial r}\left(r^2\frac{\partial Z}{\partial r}\right) + \frac{1}{r^2\sin\theta}\frac{\partial}{\partial\theta}\left(\sin\theta\frac{\partial Z}{\partial\theta}\right)\right], \quad (3)$$

$$\frac{\partial \tilde{Z}}{\partial \tilde{\tau}} = \frac{1}{r^2}\frac{\partial}{\partial r}\left(r^2\frac{\partial \tilde{Z}}{\partial r}\right) + \frac{1}{r^2\sin\theta}\frac{\partial}{\partial\theta}\left(\sin\theta\frac{\partial \tilde{Z}}{\partial\theta}\right), \quad (4)$$

where we have used the standard notation $\partial(\ ,\ )/\partial(\ ,\ )$ to represent the Jacobian and a tilde to denote the sphere interior. The operator E^2 employed in equations (1) and (2) has been defined as

$$E^2 \equiv \frac{\partial^2}{\partial r^2} + \frac{\sin\theta}{r^2}\frac{\partial}{\partial\theta}\left(\frac{1}{\sin\theta}\frac{\partial}{\partial\theta}\right). \quad (5)$$

The stream function introduced above satisfies the continuity equation. Thus, it follows that

$$\mathbf{u} = \frac{\mathbf{e}_r}{r^2\sin\theta}\frac{\partial\psi}{\partial\theta} - \frac{\mathbf{e}_\theta}{r\sin\theta}\frac{\partial\psi}{\partial r}. \quad (6)$$

In equations (1) to (5) we have nondimensionalized the variables as follows:

$$\left.\begin{aligned} r^* &= \frac{r}{R}, \quad \tau = \frac{tU_\infty}{R}, \quad \tilde{\tau} = \frac{t\tilde{\alpha}}{R^2} \\ Z^* &= \frac{Z - Z_\infty}{Z_0 - Z_\infty}, \quad \psi^* = \frac{\psi}{R^2U_\infty}, \quad \zeta^* = \frac{\zeta R}{U_\infty} \\ \mathbf{u}^* &= \frac{\mathbf{u}}{U_\infty}, \quad Re = \frac{2\rho U_\infty R}{\mu}, \\ Pe &= \frac{2U_\infty R}{\alpha}, \quad Gr = \frac{4g\beta(Z_0 - Z_\infty)R^3}{\nu^2} \end{aligned}\right\}, \quad (7)$$

where an asterisk has been used to indicate dimensionless quantities and has been dropped in the above equations. Note that the two time scales are related by $\tau = (Pe/\Phi_\alpha)\tilde{\tau}$.

The boundary conditions which accompany equations (1)–(3) include the following:

I. Axisymmetry: At the axis of symmetry, it is required that

$$\psi(\tau, r, 0) = \psi(\tau, r, \pi) = \zeta(\tau, r, 0) = \zeta(\tau, r, \pi) = 0, \quad (8)$$

$$Z(\tau, r, 0) = Z(\tau, r, \pi) = \tilde{Z}(\tilde{\tau}, r, 0) = \tilde{Z}(\tilde{\tau}, r, \pi) = 0. \quad (9)$$

II. Far-field: The stream function and temperature of the continuous phase approach the free-stream values asymptotically, i.e.

$$\lim_{r\to\infty}\psi(\tau, r, \theta) \to r^2\int_{\cos\theta}^{1} P_1(z)\,dz, \quad (10)$$

$$\lim_{r\to\infty} Z(\tau, r, \theta) \to 0, \quad (11)$$

where r_∞ is the radial distance beyond which the free-stream condition prevails.

III. Solid–fluid interface: The necessary requirements at the sphere surface include the zero normal and tangential velocity components. In addition, con-

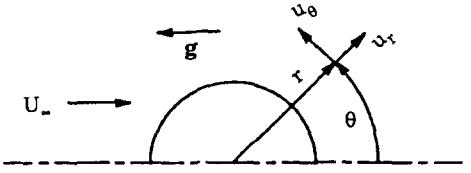

FIG. 1. Coordinate system.

tinuity of temperature and heat flux, provided no interfacial resistance exists, are also enforced. These lead to the following constraints:

$$\frac{\partial\psi}{\partial r}(\tau,1,\theta)=0,\quad \frac{\partial\psi}{\partial\theta}(\tau,1,\theta)=0, \tag{12}$$

$$Z(\tau,1,\theta)=\tilde{Z}(\tilde{\tau},1,\theta),\quad \frac{\partial Z}{\partial r}(\tau,1,\theta)=\Phi_\kappa\frac{\partial\tilde{Z}}{\partial r}(\tilde{\tau},1,\theta), \tag{13}$$

where Φ's are the property ratios of the sphere to the outside fluid.

IV. Sphere center: Temperature must be bounded,

$$\lim_{r\to 0}\tilde{Z}(\tilde{\tau},r,\theta)=\text{finite}. \tag{14}$$

To complete the problem specification, the initial conditions are taken such that

$$\psi(0,r,\theta)=0,\quad \zeta(0,r,\theta)=0, \tag{15}$$

$$Z(0,r,\theta)=0,\quad \tilde{Z}(0,r,\theta)=1. \tag{16}$$

In what follows, a hybrid numerical method that combines various approaches of weighted residual principles is described for simulating the aforementioned system of equations.

3. METHOD OF SOLUTION

For ease of numerical calculations, the domain of the continuous phase is first truncated to r_∞, then the resulting domain together with that of the dispersed phase are mapped onto $[-1, 1]$. Such projection is accomplished by means of the following coordinate transformations:

$$z=\cos\theta,\quad r=\begin{cases}\frac{1}{2}(1+\xi), & r\in[0,1]\\ \mathrm{e}^{l/2(1+\eta)}, & r\in[1,r_\infty]\end{cases} \tag{17}$$

where l is a parameter that controls the domain truncation. The deployment of the exponential mapping allows the grid points to be clustered near the sphere surface where thin boundary layers are expected to exist. Others, algebraic and tangent function mappings for example, have also been used for boundary layer type of problems; however, the exponential map seems to be a popular choice especially for the problem under consideration.

Following earlier work on spectral methods [3, 14], the dependent variables are represented as series of products of Legendre, $P_n(z)$, and Chebyshev, $T_i(\eta)$, polynomials. That is,

$$\{\zeta,\psi\}=\sum_{n=1}^{\mathcal{N}}\sum_{i=0}^{\mathcal{I}}\{a_{ni}(\tau),b_{ni}(\tau)\}\times\left\{T_i(\eta)P_n^1(z),\,T_i(\xi)\int_z^1 P_n(z^*)\,\mathrm{d}z^*\right\}, \tag{18}$$

$$\{Z,r\tilde{Z}\}=\sum_{n=0}^{\mathcal{N}}\sum_{i=0}^{\mathcal{I}}\{c_{ni}(\tau),\tilde{c}_{ni}(\tilde{\tau})\}\{T_i(\eta),T_i(\xi)\}P_n(z), \tag{19}$$

in which a's, b's, c's, $\tilde{c}$'s are the spectral coefficients of the corresponding dependent variable being expanded. As seen from equation (19), we have expanded $r\tilde{Z}$ instead of $\tilde{Z}$ alone for the sole purpose of avoiding the complications introduced by the temperature boundary conditions at the center of the particle.

Upon substitution of equations (18) and (19) into equations (1)–(4), then making use of the orthogonality properties and recursive formulas of Legendre functions, the equations become free of angular dependence. Following the weighted residual principles, the resulting equations are further simplified by forcing them to be error free at the Gauss–Lobatto points, herein referred to as collocation points, to yield a system of nonlinear equations written in iterative form as

$$\frac{\zeta_{nk}^{m+1}}{\Delta\tau}-\frac{2\,\mathrm{e}^{-l(1+\eta_k)}}{Re}\left\{\sum_{k'=0}^{NT}\left(\frac{4}{l^2}\hat{G}_{kk'}^{(2)}+\frac{2}{l}\hat{G}_{kk'}^{(1)}\right)\zeta_{nk'}^{m+1}-n(n+1)\zeta_{nk}^{m+1}\right\}=\frac{\zeta_{nk}^{*}}{\Delta\tau}+S_{nk}^{m}, \tag{20}$$

$$\sum_{k'=0}^{NT}\left(\frac{4}{l^2}\hat{G}_{kk'}^{(2)}-\frac{2}{l}\hat{G}_{kk'}^{(1)}\right)\psi_{nk'}^{m+1}-n(n+1)\psi_{nk}^{m+1}=-\mathrm{e}^{3l(1+\eta_k)/2}n(n+1)\zeta_{nk}^{m+1}, \tag{21}$$

$$\frac{Z_{nk}^{m+1}}{\Delta\tau}-\frac{2\,\mathrm{e}^{l(1+\eta_k)}}{Pe}\times\left\{\sum_{k'=0}^{NK}\left(\frac{4}{l^2}\hat{G}_{kk'}^{(2)}+\frac{2}{l}\hat{G}_{kk'}^{(1)}\right)Z_{nk'}^{m+1}-n(n+1)Z_{nk}^{m+1}\right\}=\frac{Z_{nk}^{*}}{\Delta\tau}+H_{nk}^{m}, \tag{22}$$

$$\frac{\tilde{Z}_{nk}^{m+1}}{\Delta\tilde{\tau}}-4\left\{\sum_{k'=0}^{NT}\hat{G}_{kk'}^{(2)}\tilde{Z}_{nk'}^{m+1}-\frac{n(n+1)}{(1+\xi_k)^2}n(n+1)\tilde{Z}_{nk}^{m+1}\right\}=\frac{\tilde{Z}_{nk}^{*}}{\Delta\tilde{\tau}}, \tag{23}$$

where we have used a first-order backward Euler difference to approximate the time derivatives. In the above equations (20)–(23), $\hat{G}_{k,j}^{(i)}$ is the $(NT+1)\times(NT+1)$ Chebyshev matrix representing the ith derivative [15]. Unless otherwise specified, the asterisk denotes the previous time level and those without it pertain to the current level.

The convective terms in equations (20) and (22) may be expressed as

$$S_{nk}=\frac{-2}{l}\mathrm{e}^{-3l(1+\eta_k)/2}\sum_{i=1}^{NL}\sum_{j=1}^{NL}\left\{\omega_{ij}^{n}\psi_{ik}\left(\sum_{k'=0}^{NT}\hat{G}_{kk'}^{(1)}\zeta_{jk'}-\frac{l}{2}\zeta_{jk}\right)+\chi_{ij}^{n}\zeta_{jk}\sum_{k'=0}^{NT}\hat{G}_{kk'}^{(1)}\Psi\psi_{ik'}\right\}+\frac{Gr}{Re^2}\times\mathrm{e}^{l(1+\eta_k)/2}\left\{\frac{2}{l}\sum_{i=0}^{NL}\sum_{k'=0}^{NT}\omega_{i1}^{n}\hat{G}_{kk'}^{(1)}Z_{ik'}-\sum_{i=0}^{NL}\omega_{1i}^{n}Z_{ik}\right\}, \tag{24}$$

$$H_{nk} = \frac{-2}{l} e^{-3l(1+\eta_k)/2} \sum_{i=0}^{NL} \sum_{j=1}^{NL} \left\{ \lambda_{ij}^n \psi_{jk} \sum_{k'=0}^{NT} \hat{G}_{kk'}^{(1)} Z_{ik'} + \gamma_{ij}^n Z_{ik} \sum_{k'=0}^{NT} \hat{G}_{kk'}^{(1)} \psi_{jk'} \right\}, \quad (25)$$

with the coefficients ω_{ij}^n, χ_{ij}^n, λ_{ij}^n, and γ_{ij}^n given by

$$\omega_{ij}^n = -(2n+1) \left[\frac{j(j+1)}{n(n+1)} \right]^{1/2} \times \begin{pmatrix} n & i & j \\ -1 & 0 & 1 \end{pmatrix} \begin{pmatrix} n & i & j \\ 0 & 0 & 0 \end{pmatrix}, \quad (26)$$

$$\chi_{ij}^n = (2n+1) \left[\frac{j(j^2-1)(j+2)}{n(n+1)i(i+1)} \right]^{1/2} \times \begin{pmatrix} n & i & j \\ -1 & -1 & 2 \end{pmatrix} \begin{pmatrix} n & i & j \\ 0 & 0 & 0 \end{pmatrix}, \quad (27)$$

$$\lambda_{ij}^n = \frac{2n+1}{2} \begin{pmatrix} n & i & j \\ 0 & 0 & 0 \end{pmatrix} \begin{pmatrix} n & i & j \\ 0 & 0 & 0 \end{pmatrix}, \quad (28)$$

$$\gamma_{ij}^n = \frac{-(2n+1)}{2} \left[\frac{j(j+1)}{i(i+1)} \right]^{1/2} \times \begin{pmatrix} n & i & j \\ 0 & 1 & -1 \end{pmatrix} \begin{pmatrix} n & i & j \\ 0 & 0 & 0 \end{pmatrix}, \quad (29)$$

where

$$\begin{pmatrix} j_1 & j_2 & j_3 \\ m_1 & m_2 & m_3 \end{pmatrix}$$

has been termed the 3-J coefficient in the mathematical literature. Procedures to numerically compute these integrals were discussed by Rottenberg *et al.* [16] and interested readers are referred to their monograph.

One of the difficulties arising in solving equations (20)–(23) is due to the absence of the vorticity boundary conditions. However, the decomposition concept has proven effective as Nguyen and Chung [14] applied it to flow past an impulsively started sphere. Since the solution technique to the Navier–Stokes equations has been discussed at length, and furthermore the flow is now decoupled with heat transfer, only methods used in the energy equations are described in detail.

To begin the discussion, the solution of each component of temperature at any iteration cycle, say n and m respectively, is sought as a linear combination of the solutions of the supplementary problems, i.e.

$$\begin{Bmatrix} Z_n^m \\ \tilde{Z}_n^m \end{Bmatrix} = \begin{Bmatrix} \Xi_0 \\ \tilde{\Xi}_0 \end{Bmatrix} + \phi_1 \begin{Bmatrix} \Xi_1 \\ 0 \end{Bmatrix} + \phi_2 \begin{Bmatrix} 0 \\ \tilde{\Xi}_1 \end{Bmatrix}, \quad (30)$$

where ϕ_1 and ϕ_2 are the unknown coefficients to be determined from the interfacial boundary conditions: temperature and heat flux continuities. In the transformed coordinates, expressions (13) form a linear system of two equations in two unknowns written in matrix notation as

$$\begin{bmatrix} \frac{2}{l\Phi_\kappa} \Xi_1'|_{\eta=-1} (-2\tilde{\Xi}_1' + \tilde{\Xi}_1)|_{\xi=1} \\ \Xi_1|_{\eta=-1} - \tilde{\Xi}_1|_{\xi=1} \end{bmatrix} \begin{Bmatrix} \phi_1 \\ \phi_2 \end{Bmatrix} = \begin{Bmatrix} (2\tilde{\Xi}_0' - \tilde{\Xi}_0)|_{\xi=1} - \frac{2}{l\Phi_\kappa} \Xi_0'|_{\eta=-1} \\ \tilde{\Xi}_0|_{\xi=1} - \Xi_0|_{\eta=-1} \end{Bmatrix}, \quad (31)$$

in which the prime represents derivative operator.

Among several existing direct and indirect methods to treat the boundary value problems, iterative algorithms seem to offer many advantages with respect to the computing time and the memory storage. Hence, we shall adopt the following procedure, based on the ideas of successive substitution which is selected for simplicity, which consists of four steps in advancing from one time level to the next.

A. Solve for Ξ's and $\tilde{\Xi}$'s according to the following auxiliary problems:

$$\left. \begin{aligned} \frac{\Xi_{ik}}{\Delta\tau} - \frac{2e^{-l(1+\eta_k)}}{Pe} \left[\sum_{k'=0}^{NT} \left(\frac{4}{l^2} \hat{G}_{kk'}^{(2)} + \frac{2}{l} \hat{G}_{kk'}^{(1)} \right) \Xi_{ik'} - n(n+1)\Xi_{ik} \right] &= \left(\frac{Z_{nk}^*}{\Delta\tau} + H_{nk} \right) \delta_{0i} \\ \text{with} \quad \Xi_{i0} = 0 \quad \text{and} \quad \Xi_{i\widetilde{NT}} &= \delta_{1i} \end{aligned} \right\}, \quad i = 0, 1, \quad (32)$$

$$\left. \begin{aligned} \frac{\tilde{\Xi}_{ik}}{\Delta\tilde{\tau}} - 4 \left[\sum_{k'=0}^{NT} \hat{G}_{kk'}^{(2)} \tilde{\Xi}_{ik'} - \frac{n(n+1)}{(1+\xi_k)^2} \tilde{\Xi}_{ik} \right] &= \frac{\tilde{Z}_{nk}^*}{\Delta\tilde{\tau}} \delta_{0i} \\ \text{with} \quad \tilde{\Xi}_{i0} = 0 \quad \text{and} \quad \tilde{\Xi}_{i\widetilde{NT}} &= \delta_{1i} \end{aligned} \right\}, \quad i = 0, 1. \quad (33)$$

B. Solve equation (31) for the decomposing coefficients ϕ_1 and ϕ_2.

C. Compute new estimates using equation (30) and check for convergence on the basis of the following criteria:

$$|X^{m+1} - X^m| \leqslant \{\varepsilon\}, \quad (34)$$

where $X = \{\zeta_{n0}, \ldots, \zeta_{nNT}, \psi_{n0}, \ldots, \psi_{nNT}, Z_{n0}, \ldots, Z_{nNT}, \tilde{Z}_{n0}, \ldots, \tilde{Z}_{nNT}\}^T$ and $\{\varepsilon\}$ is a prescribed tolerance vector. In case such conditions are not satisfied, the flow field and the convective terms are then updated and steps A, B, and C are repeated.

It is appropriate to add a remark that step A involves equations with the left-hand sides unchanged with time. Hence, the matrices may be factored into upper and lower matrices once and for all. As a preliminary assessment of the above algorithm, convergence history indicates that the desired tolerance

(default value is 0.001) is reached within one or two iterations except for the first few time levels.

4. PHYSICAL QUANTITIES

Besides the detailed histories of the evolution of thermal process, a number of quantities are of importance in this article. Of particular interest are the drag coefficient for fluid flow and the heat transfer rate for energy transport. Also of relevance in this study are the interfacial quantities which are subjected to significant effects augmented by natural convection. Because these lend themselves to a better understanding of combined convection heat transfer, a derivation is given below.

Two main contributions to the total drag force are the form and the viscous drags. When normalized with the inertial force $(\pi\rho U_\infty^2 R^2)$, there results the drag coefficient [14],

$$C_D = -2\int_{-1}^{1} \Pi|_{\eta=-1} z\,dz - \frac{4}{Re}\int_{-1}^{1} \zeta|_{\eta=-1}\sqrt{(1-z^2)}\,dz = \frac{-8}{3\,Re}\left(\zeta_{1NT} - \frac{2}{l}\sum_{k=0}^{NT} \hat{G}^{(1)}_{NTk}\zeta_{1k}\right). \quad (35)$$

By defining the particle temperature as the volume-averaged temperature, one deduces the equation

$$Z_b(\tilde{\tau}) = \frac{3}{2}\int_0^1\int_{-1}^{1} \tilde{Z}(\tilde{\tau},\xi,z) r^2\,dr\,dz \quad (36)$$
$$= \frac{3}{4}\sum_{i=0}^{\widetilde{NT}} \tilde{c}_{0i}(\tilde{\tau})\int_{-1}^{1}(1+\xi)T_i(\xi)\,d\xi.$$

The local surface temperature can be computed from the equation,

$$Z_s(\tilde{\tau},\theta) = \sum_{n=0}^{NL} \tilde{Z}_{n0}P_n(z), \quad (37)$$

and its average can easily be verified to be $\bar{Z}_s(\tilde{\tau}) = \tilde{Z}_{00}(\tilde{\tau})$.

The instantaneous local Nusselt number gives a direct measure of heat transfer rate and is computed from the definition:

$$Nu(\tau,\theta) = -\left(\frac{4}{l\tilde{Z}_b}\right)\frac{\partial Z}{\partial\eta}\bigg|_{\eta=-1} = \frac{-4}{l\tilde{Z}_b}\sum_{n=0}^{NL}\sum_{k=0}^{NT} \hat{G}^{(1)}_{NTk}Z_{nk}P_n(z). \quad (38)$$

The overall Nusselt number can be obtained by integrating equation (38) over the entire surface area of the sphere. Upon performing the integration with the aid of the orthogonality property of the Legendre function, the mean Nusselt number becomes

$$Nu_m(\tau) = \frac{-4}{l\tilde{Z}_b}\sum_{k=0}^{NT} \hat{G}^{(1)}_{NTk}Z_{0k}(\tau). \quad (39)$$

In subsequent discussion, the heat transfer process will be examined in greater detail, and the quantities derived in this section will be used to assist in interpreting the simulation results.

5. RESULTS AND DISCUSSION

To illustrate the salient features of the present approach, this section is divided into two parts. In the first part we shall study the evolution of the temperature and the flow fields of a system in which a sand (cork ground) particle travels in air. The thermophysical properties of this system are taken at an effective temperature (100 F) so that $Pr = 0.7$, $\Phi_\kappa = 1.333$, and $\Phi_\alpha = 5\times10^{-3}$. In the second part, we shall examine the local behavior of interfacial quantities such as the Nusselt number, the surface vorticity, the surface pressure, and the surface temperature while Gr varies. Along the same line we shall pursue a parametric study to examine the time histories of Nusselt number and drag coefficient for a wide range of Re and Gr. Throughout the study, values of NL and NT are set to be 15 and 120 respectively with a time increment of 0.001. The truncation radius r_∞ is fixed at 30 to ensure proper convergence.

Figures 2(a)–(c) and 3(a)–(c) are respectively the temporal developments of the velocity and temperature fields for $Re = 80$ at $\tau = 0.2$, 2, and 10. As for the flow field, it started with a pattern resembling the potential flow (Fig. 2(a)) because the viscous actions are limited to a very thin hydrodynamic boundary layer at the surface. As time proceeds, this layer grows in thickness and a wake is formed behind the sphere, as clearly demonstrated in Figs. 2(a) and (b), which is a precursor to the development of an eddy. Once triggered, the eddy volume expands continuously with time. At $\tau = 10$, the eddy length is already longer than the sphere diameter as shown in Fig. 2(c). With regard to the temperature distribution, spherical symmetry is seen in Fig. 3(a) indicating a conduction dominance in the early stage of the heat transfer process. Such an attribute may or may not last long depending on the convection intensity because once convection overwhelms diffusion, the structure of the temperature field is modified in a manner such that the isotherms elongate in the stream-wise direction (see Figs. 3(b) and (c)). The main action of the convective mechanism is to carry the warm fluid away from the hot surface and leave behind fresh fluid, thereby, maintaining the highest thermal potential gradient possible for heat flow.

The results presented thus far do not reflect the effects due to gravity-induced flow. Because such effects are likely confined to a zone near the particle, it is wise to consider various interfacial quantities. Figures 4(a) and (b) are the respective surface pressure and vorticity at three different values of Grashof num-

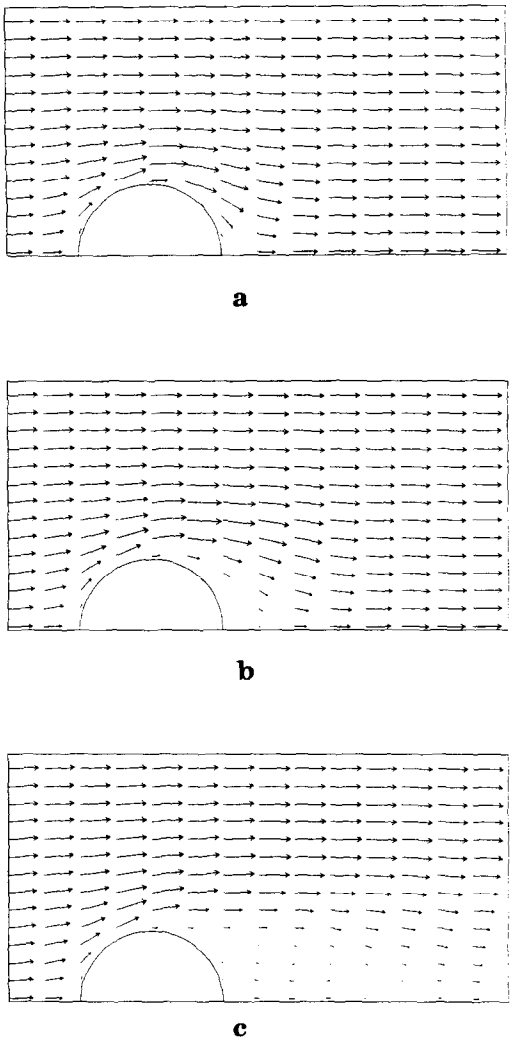

FIG. 2. Velocity vectors: (a) $\tau = 0.2$, (b) $\tau = 2$, and (c) $\tau = 10.0$ ($Re = 80$, $Gr = 10^5$, $Pr = 0.7$, $\Phi_\alpha = 5 \times 10^{-3}$, $\Phi_\kappa = 1.333$).

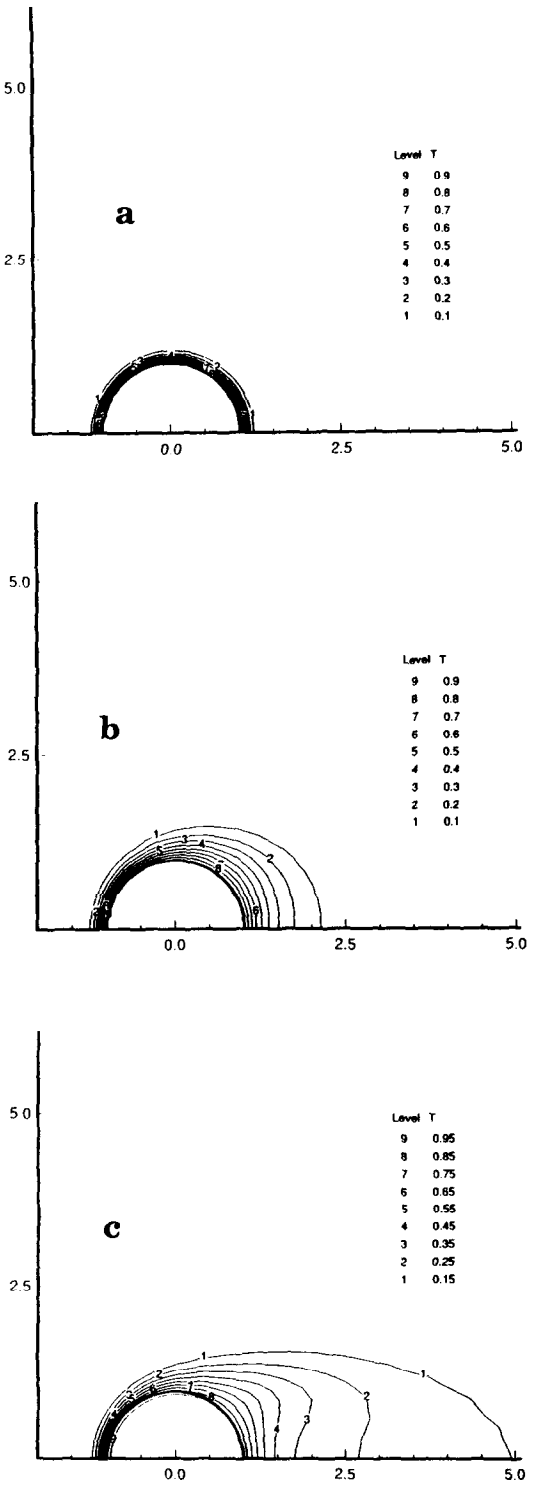

FIG. 3. Temperature contours: (a) $\tau = 0.2$, (b) $\tau = 2$, and (c) $\tau = 10$ ($Re = 80$, $Gr = 10^5$, $Pr = 0.7$, $\Phi_\alpha = 5 \times 10^{-3}$, $\Phi_\kappa = 1.333$).

bers: -10^5, 0, and 10^5 where the negative sign indicates the buoyancy-induced flow and the free stream are in the same direction. In general, free convection is most influential in the wake region where significant effects are observed, as confirmed in Figs. 4(a) and (b), and are weakened when moving toward the front stagnation point. Also obvious from these figures are that the surface pressure and vorticity are dependent upon the direction of the buoyancy; they experience an increase if the buoyancy aids the main flow and a decrease otherwise. It is this behavior which substantiates the fact that free convection flow greatly affects the flow structure especially in the wake. Figures 4(a) and (d) demonstrate similar effects on the temperature field.

The net effect on the transient drag is plotted in Figs. 5(a)–(c) for $Pr = 0.7$ and $\Phi_\alpha = 1$ with different sets of values of (Gr, Re and Φ_κ). The value of Φ_α so selected is based on two considerations: first, there exists an equation, applicable only when $\Phi_\alpha = 1$, to approximate the conjugate heat transfer rates from the information of the internal and external problems. Second, there also exists an application, such as in

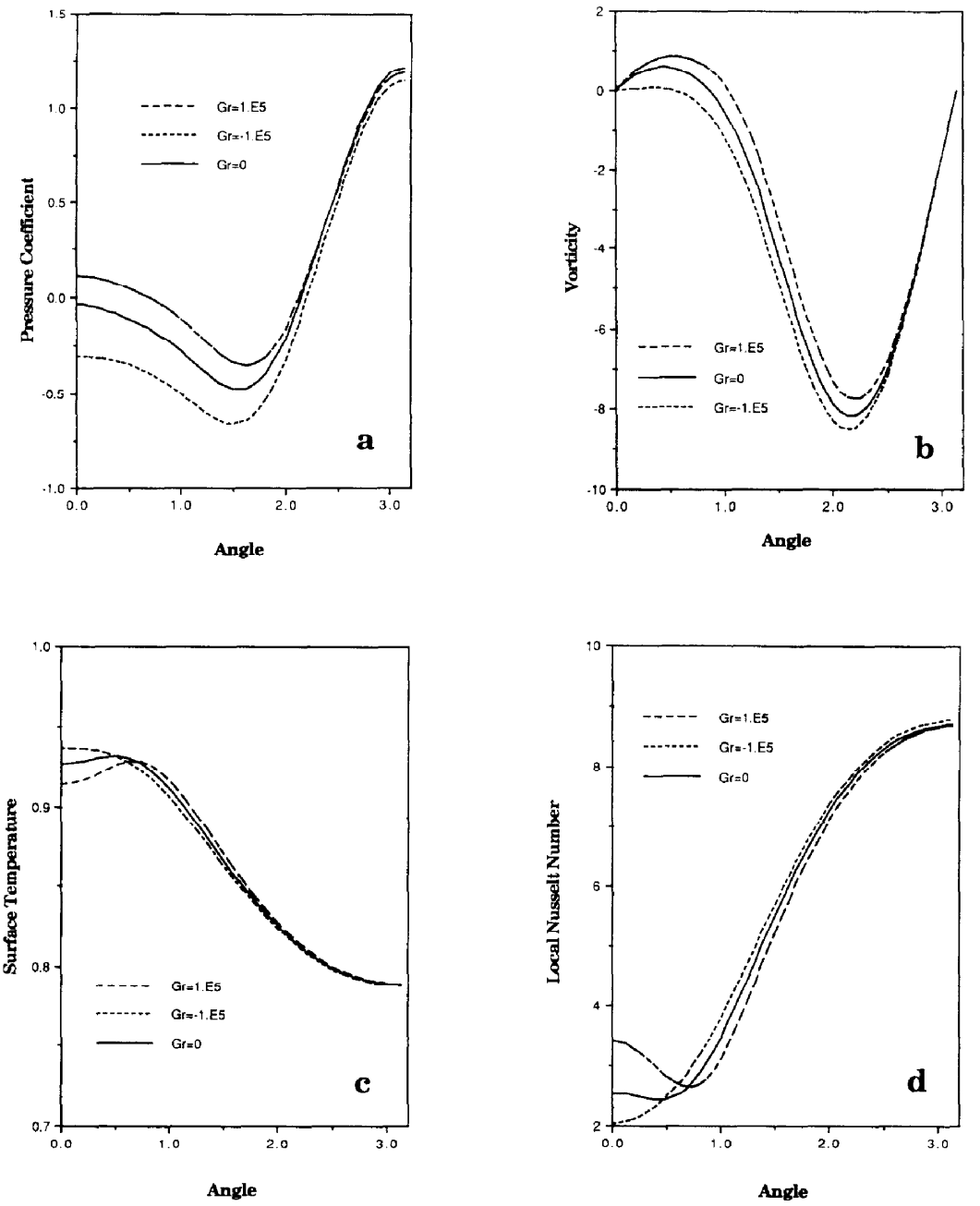

FIG. 4. Effects of free convection on: (a) surface pressure, (b) surface vorticity, (c) surface temperature, and (d) local Nusselt number ($Re = 80$, $Pr = 0.7$, $\Phi_g = 5 \times 10^{-3}$, $\Phi_k = 1.333$).

thermal plasmas processing where a water droplet is injected into a helium gas stream, for which Φ_g is of the order of unity. Qualitatively, diffusion controls the momentum transport at small times; thus, the total drag is practically unaffected regardless of how strong the buoyancy force is. Nonetheless, it appears that if the buoyancy-induced motion is strong enough and is in the same direction as the free stream, it could drive the low pressure zone away from the trailing surface, thereby delaying the formation of the eddy current. Due to this alteration of the flow field, the total drag is lower than the corresponding forced flow. When they are in the opposite direction, the main flow is decelerated and the wake is therefore reduced in size causing the drag force to increase. To quantify the increase/decrease in drag force, the asymptotic drag was normalized by the value obtained in pure forced convection and the results are tabulated in Table 1. A quick glance at the table indicates that motion induced by density variations only produces minor effects

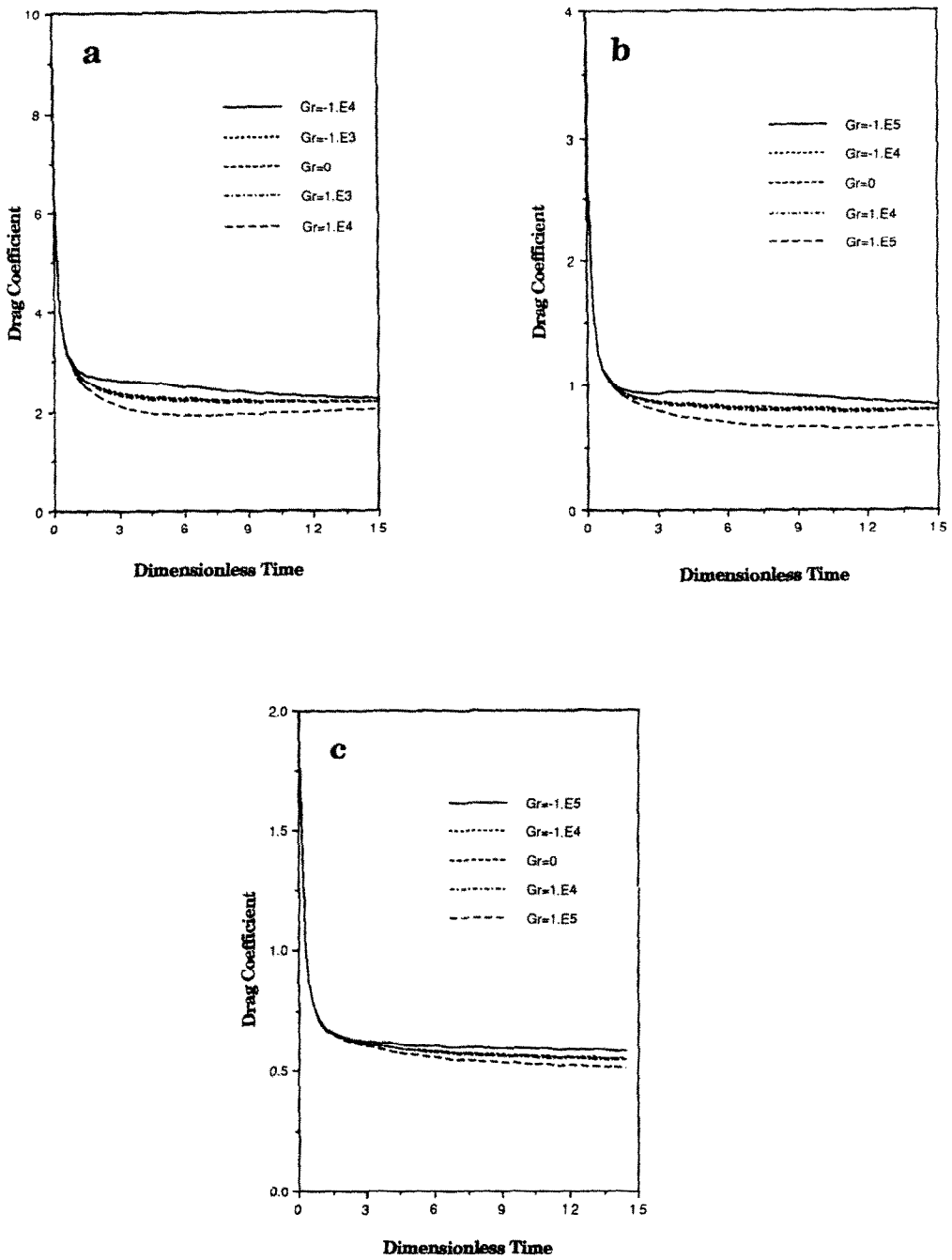

FIG. 5. Effects of free convection on drag coefficient with $Pr = 0.7$ and $\Phi_\alpha = 1$: (a) $Re = 10$ and $\Phi_\kappa = 0.333$, (b) $Re = 10$ and $\Phi_\kappa = 1$, and (c) $Re = 10$ and $\Phi_\kappa = 3$.

unless the ratio Gr/Re^2 is greater than 10, which corresponds to a change of nearly 7% in the drag coefficient. The present finding is consistent with the conclusion drawn by Wong *et al.* [12].

To see how the overall heat transfer rate is influenced, Figs. 6(a)–(c) are presented for different values of $|Gr|$ ranging from 0 to 10^5. As one may anticipate, the mean Nusselt numbers are indistinguishable in the limit as $\tau \to 0$ which is explained by the fact that conduction is the primary transfer mechanism in the early stage of the heat transfer process. During this period, the Nusselt number varies linearly with time; however, if sufficient time is allowed, convection becomes more intensified and as a result, the slope of the transient Nusselt number curve changes. Accompanying these figures is Table 2 where the values are normalized with the corresponding value in pure forced convection. Like the drag coefficient,

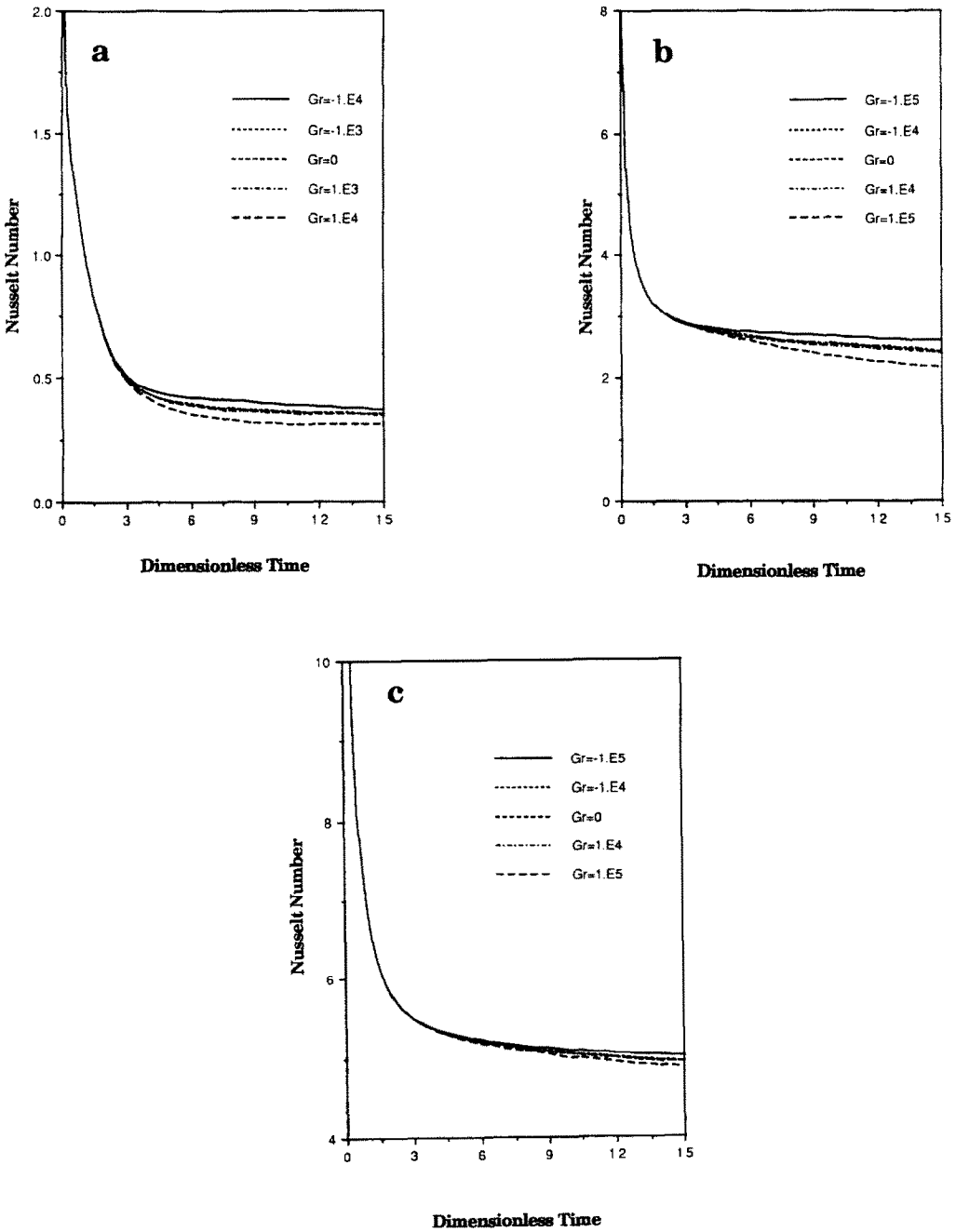

FIG. 6. Effects of free convection on Nusselt number with $Pr = 0.7$ and $\Phi_\alpha = 1$: (a) $Re = 10$ and $\Phi_\kappa = 0.333$, (b) $Re = 10$ and $\Phi_\kappa = 1$, and (c) $Re = 10$ and $\Phi_\kappa = 3$.

Gr/Re^2 has to be at least of the order of 10 before natural convection can either promote or degrade the heat transfer rate.

In an effort to provide confidence to the results reported above, Tables 3 and 4 are prepared for Nusselt number and drag coefficient comparisons. Because of the lack of data for conjugate problems on mixed convection, we shall restrict ourselves to limiting cases where data are either available or can be estimated. For the Nusselt numbers, our results are slightly higher than those of Oliver and Chung [17], but the differences are within one percent. Also tabulated are those computed from the following equation:

$$Nu_{\text{conj}} = \left(\frac{1}{\Phi_\kappa \overline{Nu}_{\text{int}}} + \frac{1}{Nu_{\text{ext}}} \right)^{-1}, \tag{40}$$

which has been proposed for estimating the conjugate

Table 1. Late-time drag coefficient ratio ($\tau = 15$)

	(Re, Φ_κ)		
Gr	(10, 0.333)	(50, 1)	(100, 3)
-10^5	—	1.057	1.062
-10^4	1.031	1.010	1.007
-10^3	1.004	1.001	1.001
0	1.0	1.0	1.0
10^3	0.995	0.999	0.999
10^4	0.935	0.989	0.993
10^5	—	0.833	0.934

Table 2. Late-time Nusselt number ratio ($\tau = 15$)

	(Re, Φ_κ)		
Gr	(10, 0.333)	(50, 1)	(100, 3)
-10^5	—	1.080	1.015
-10^4	1.053	1.005	1.001
-10^3	1.007	1.0	1.0
0	1.0	1.0	1.0
10^3	0.992	0.999	1.0
10^4	0.889	0.994	0.998
10^5	—	0.895	0.986

Table 3. Asymptotic Nusselt number comparison ($Re = 20$, $Pe = 300$, $Gr = 0$, $\Phi_\alpha = 1$)

Φ_κ	Present	Ref. [17]	Equation (40)
0.333	1.99	1.84	1.78
1.0	4.19	4.08	3.89
3.0	6.83	6.72	6.41

Table 4. Asymptotic drag coefficient comparison ($Gr = 0$)

Ref.	$Re = 10$	$Re = 50$	$Re = 100$
Present	2.161	0.802	0.546
Clift *et al.* [1]	2.076	0.769	0.546

Nusselt number from those corresponding to internal and external problems. For the drag coefficients, the present predictions are compared against the correlation of Schiller and Nauman as compiled by Clift *et al.* [1]. Again, exceptional agreement was obtained. According to Clift and his associates, the Schiller and Nauman correlation is reliable within a −5–4% error range.

Acknowledgement—The authors are indebted to Dr Rodney Douglas of the Computational Fluid Dynamics Unit of EG&G Idaho, Inc. for his review and helpful comments. This work was performed under the auspices of the U.S. Department of Energy, contract DE-AC07-76-ID01570, and was supported in part by the INEL Long-Term Research Initiatives Program in Computational Mechanics.

REFERENCES

1. R. Clift, J. R. Grace and M. E. Weber, *Bubbles, Drops, and Particles*, Chaps. 3 and 5. Academic Press, New York (1978).
2. S. C. R. Dennis, J. D. A. Walker and J. D. Hudson, Heat transfer from a sphere at low Reynolds numbers, *J. Fluid Mech.* **60,** 273–283 (1973).
3. S. Paik, H. D. Nguyen and J. N. Chung, Transient conjugated heat transfer analysis from a sphere: A direct simulation, submitted to *J. Comput. Phys.*
4. N. Riley, The heat transfer from a sphere in free convection flow, *Comput. Fluids* **14,** 225–237 (1986).
5. T. Fujii, M. Fujii and T. Honda, A numerical analysis of laminar free convection around an isothermal sphere, *Numer. Heat Transfer* **4,** 69–84 (1981).
6. T. Fujii, T. Honda and M. Fujii, A numerical analysis of laminar free convection around an isothermal sphere: Finite-difference solution of the full Navier–Stokes and energy equations between concentric sphere, *Numer. Heat Transfer* **7,** 103–111 (1984).
7. D. B. Ingham, Heat transfer by natural convection between spheres and cylinders, *Numer. Heat Transfer* **4,** 53–67 (1981).
8. F. Geoola and A. R. H. Cornish, Numerical solution of steady-state free convective heat transfer from a solid sphere, *Int. J. Heat Mass Transfer* **24,** 1369–1379 (1981).
9. C. A. Hieber and B. Gebhart, Mixed convection from a sphere at small Reynolds and Grashof numbers, *J. Fluid Mech.* **38,** 137–159 (1969).
10. A. Acrivos, On the combined effect of forced and free convection heat transfer in laminar boundary layer flows, *Chem. Engng Sci.* **21,** 343–352 (1966).
11. T. S. Chen and A. Mucoglu, Analysis of mixed forced and free convection about a sphere, *Int. J. Heat Mass Transfer* **20,** 867–875 (1977).
12. K. L. Wong, S. C. Lee and C. K. Chen, Finite element solution of laminar combined convection from a sphere, *J. Heat Transfer* **108,** 860–865 (1986).
13. D. L. R. Oliver and J. N. Chung, Conjugate unsteady heat transfer of a translating droplet at low Reynolds number, *Int. J. Heat Mass Transfer* **29,** 879–887 (1986).
14. H. D. Nguyen and J. N. Chung, A Chebyshev–Legendre spectral method for the transient solutions of flow past a solid sphere, *J. Comput. Phys.* **104,** 303–312 (1993).
15. H.-C. Ku and D. Hatziavramidis, Solution of the two-dimensional Navier–Stokes equations by Chebyshev expansion methods, *Comput. Fluids* **13,** 99–113 (1985).
16. M. Rottenberg, R. Bivins, N. Metropolis and J. K. Wooten, *The 3-J and 6-J Symbols*. MIT Press, Cambridge (1959).
17. D. L. R. Oliver and J. N. Chung, Unsteady conjugate heat transfer from a translating fluid sphere at moderate Reynolds numbers, *Int. J. Heat Mass Transfer* **33,** 401–408 (1990).